3D Spectroscopy of Blue Compact Galaxies. Diagnostic Diagrams

Ismael Martínez-Delgado[1] , Guillermo Tenorio-Tagle[2], Casiana Muñoz-Tuñón[1], Alexei V. Moiseev[3]

and

Luz M. Cairós[4]

Instituto de Astrofísica de Canarias, Vía Láctea, E-38200 La Laguna, Tenerife, Canary Islands, Spain;

idelgado@iac.es, cmt@iac.es

Instituto Nacional de Astrofísica, Óptica y Electrónica, AP 51, 72000 Puebla, Mexico;

gtt@inaoep.mx

Special Astrophysical Observatory, 369167 Nizhnij Arkhyz, Russia;

moisav@sao.ru

Astrophysikalisches Institut Postdam, An der Sternwarte 16, D-14482 Potsdam, Germany;

luzma@aip.de

ABSTRACT

Here we present the analysis of 3D spectroscopic data of three Blue Compact Galaxies (Mrk 324, Mrk 370, and III Zw 102). Each of the more than 22500 spectra obtained for each galaxy has been fitted by a single gaussian from which we have inferred the velocity dispersion (σ), the peak intensity (I_{peak}), and the central wavelength (λ_c). The analysis shows that the σ *vs* I_{peak} diagrams look remarkably similar to those obtained for giant extragalactic H II regions. They all present a supersonic narrow horizontal band that extends across all the range of intensities and that result from the massive nuclear star-forming regions of every galaxy. The σ *vs* I_{peak} diagrams present also several inclined bands of lower intensity and an even larger σ, arising from the large galactic volumes that surround the main central emitting knots. Here we also show that the σ *vs* λ_c and λ_c *vs* I_{peak} diagrams, are powerful tools able to unveil the presence of high and low mass stellar clusters, and thus allow for the possibility of inferring the star formation activity of distant galaxies, even if these are not spatially resolved.

Subject headings: galaxies: spectroscopy — galaxies: individual(Mrk 370, Mrk 324, III Zw 102) –galaxies: dwarfs — galaxies: starbursts

1. Introduction

High resolution panoramic spectroscopy with good spatial and spectral resolution is known to be a powerful tool for studying the kinematics of ionized nebulae as it leads to a simultaneous mapping, at seeing limited resolution, of a particular emission line over the whole nebula. This however can easily lead to several tens of thousands of spectra, making it difficult to issue a detailed and/or a global interpretation of the data. An analysis procedure that has proven to be simple and powerful results from fitting a single gaussian to each of the resultant emission line profiles (see Muñoz-Tuñón 1994; Muñoz-Tuñón et al. 1995). A single gaussian regardless of the actual degree of asymmetry or splitting in the line profiles. The fit is to conserve the flux of the line profile, and thus lower intensity but broader lines would result from the most asymmetric or largely splitted line profiles. From the resultant fits one can derive the velocity dispersion (σ), the peak intensity (I_{peak}) of the fitted lines as well as their central wavelength (λ_c). Such a method when applied to giant extragalactic H II region (GHIIR) data, leads to two distinct regions in the σ *vs* I_{peak} diagram (see Muñoz-Tuñón et al. 1996): A supersonic ($\sigma > c_{H\,II}$), relatively narrow horizontal band with all possible peak intensity values, and a second region populated by lower intensity points presenting even larger supersonic σ values, that crowd along multiple inclined bands. For the case of GHIIRs it has been shown (see Muñoz-Tuñón 1994; Muñoz-Tuñón et al. 1996; Sabalisck et al. 1995; Fuentes-Masip et al. 2000; Telles et al. 2001, the last reference for the case of H II Galaxies data) that the horizontal band is conformed by data with truly gaussian profiles arising mainly from the brightest portions of the nebula, from the small regions that enclose groups or clusters of stars. The inclined lower intensity and highly supersonic bands on the other hand, emanate from multiple photoionized shells that surround the star-forming centers and are likely to result from the stellar mechanical energy impact into the ISM, and thus from single gaussian fits to highly asymmetric or strongly splitted lines. The analysis of the σ *vs* I_{peak} diagram for GHIIRs in nearby galaxies (closer than 1 Mpc) was then proposed as an excellent tool to determine their degree of evolution on kinematic bases (Muñoz-Tuñón et al. 1996). Here we extend the analysis to Blue Compact Galaxies (BCGs) at even larger distances and show that they experience a similar dynamical evolution (ie. their σ *vs* I_{peak} diagrams look very much like those of GHIIRs). We further extend our analysis by looking also at the σ *vs* λ_c and λ_c *vs* I_{peak} diagrams, and show them as ideal tools to distinctly unveil the presence of high and low mass stellar clusters.

Here section 2 provides a short description of the observations. Section 3 contains a detailed analysis of the data by means of the diagnostic diagrams here proposed and section 4 gives a summary and a discussion of our findings.

2. The observations

We use the 6m Big Telescope Alta-azimuthal (BTA) of the Special Astrophysical Observatory (SAO) in Nizhnij Arkhyz (Russia), equipped with the multi-mode focal reducer SCORPIO[1] in the scanning Interferometer Fabry-Perot (IFP) observational mode (see Afanasiev & Moiseev 2005), for the observations of three BCGs: Mrk 370, III Zw 102, and Mrk 324. SCORPIO is provided with a EEV 42-40 CCD array of 2048 × 2048 pixels with an instrumental scale of 0.18 ″ pixel^{-1}. A set of interference filters centered at the Hα line, covering an interval of systemic velocities that range from −200 to 10000 km s^{-1}, is used at the IFP observational mode. The IFP offers two configuration depending on the interference order, in our case at the Hα line, the IFP260 (at the interference order 235) and the IFP500 (at the interference order 501). Our observation runs were performed using the IFP500 mode, that offers a better spectral resolution in the Ha emission line.

The output from the IFP results on a 3D data cube with x and y being the spatial plane and z the wavelength sampling or ethalon step, that in the case of IFP500 mode, it translates into 32-40 channels. The original data cube dimensions were (522,522,36) although for our analysis we reduced the size, matching the objects size, to (150,150,36). The Free Spectral Range (FSR) was 13 Å, enough to sample the Hα line, that was scanned with a spectral sampling of 0.7 Å ≈ 32 km s^{-1}. A binning of 4×4 pixels was applied in the spatial directions in order to reduce the time exposure and improve the signal to noise of the final data cube, resulting in a final spatial scale of 0.7 ″ pixel^{-1}. The instrumental width taken from a fitting of the calibration lamp data cube was $\sigma_{inst} = 20 \pm 3$ km s^{-1}. Table 1 lists a log of the observations together with some data about the galaxies: Column 1 gives the name of the object; columns 2 and 3 show the coordinates (from NED[2]); columns 4 shows the linear scale for each galaxy; column 5 lists the total time exposure of the observations; column 6 gives the seeing conditions; column 7 shows the systemic velocity of each galaxy and column 8 gives the distance in Mpc. Each of our SCORPIO trimmed data cubes contains a total of 22500 spectra from an area of ∼3 arcmin^2. The bulk of the data thus requires of automatic techniques of analysis to extract the full power of 3D spectroscopy. For each of the three galaxies, their Hα emission lines in every pixel were fitted by single gaussians, to then obtain their I_{peak}, σ, and λc, as described in Muñoz-Tuñón et al. (1995, 1996). The velocity dispersion is given in km s^{-1} and is corrected for the instrumental and thermal broadening ($\sigma^2 = \sigma^2_{obs} - \sigma^2_{inst} - \sigma^2_{th}$). We then used *MoisSoft*, the software package designed for the

[1]http://www.sao.ru/hq/lsfvo/devices/scorpio/scorpio.html

[2]NASA/IPAC Extragalactic Database is operated by the Jet Propulsion Laboratory, California Institute of Technology, under contract with the National Aeronautics and Space Administration(NASA).

manipulation of SCORPIO-IFP spectral line data cubes. For a detailed explanation about the data reduction procedure, see Moiseev (2002).

3. Three Dimensional Spectroscopy of BCDs

3.1. Mrk 324

Mrk 324 is a galaxy classified as a Blue Compact Dwarf (BCD, see Thuan & Martin 1981) and is included as a Nucleated BCD in the morphological classification of Cairos et al. (2001), as it is basically powered by a luminous central knot. The star formation history of the galaxy fits well with an instantaneous star formation law with a Salpeter IMF (α = 2.35) and a range of masses between 1$\leq M/M_{\odot} \leq$100, in which a central knot of 4.4 Myr and 1.4×10^5 M$_{\odot}$ in stars dominates 95% of the emission flux of the galaxy (see Martínez-Delgado et al. 2006).

Figure 1 (upper row of panels) shows the results from the single gaussian fit to the full Hα SCORPIO data set in the σ *vs* I$_{peak}$, σ *vs* λ_c, and λ_c *vs* I$_{peak}$ diagrams for Mrk 324. The last frame, upper row, shows the Hα image of the nucleated galaxy (see Cairós et al. 2001) obtained at the NOT 2.52m telescope of the Roque de Los Muchachos Observatory (ORM) in La Palma (Spain). The resemblance of the σ *vs* I$_{peak}$ diagram with those of GHIIRs is remarkable. It presents a horizontal band that limits the values of σ to supersonic values ($\sigma \geq$ 20 km s^{-1}) and a bunch of low intensity points at even higher σ values, that delineate a triangular structure above the horizontal band. If one selects from the σ *vs* I$_{peak}$ diagram the highest intensity data points, those belonging to the horizontal band (see second row of panels in Figure 1), these in the σ *vs* λ_c diagram appear clumped at a given λ_c ($\sim$ 6598.2 A) what implies that they all arise from a very similar location in the galaxy, that they all belong in principle to a single entity. Note however, that this is not exactly coincident with the rest wavelength of the galaxy (marked in the λ_c plots with a red line, see Figure 1). The selected points in the λ_c *vs* I$_{peak}$ diagram defined also a pointed structure towards high intensity values. These points in the emission-line peak intensity map (last frame) display their location in the galaxy, which indeed coincides with the major burst of star formation in Mrk 324. A major burst with an estimated mass in stars $\sim 4 \times 10^5$ M$_{\odot}$ and an age of about 4.4 Myr (see Martínez-Delgado 2005; Martínez-Delgado et al. 2006) that causes an H II region with a radius of $\sim$ 250 pc. On the other hand, the data belonging to the inclined bands with a higher velocity dispersion and a lower intensity in the σ *vs* I$_{peak}$ diagram (see third row of panels in Figure 1) appear well scattered in λ_c and arise from a large-scale (600 pc in thickness) expanding rim that surrounds the central emitting knot, as shown in the last panel of the third row. The inserts in the last column of Figure 1 display the Hα line and its

single gaussian fit at various locations in the galaxy. As in GHIIRs, the data corresponding to the horizontal band in the σ *vs* I_{peak} diagram leads to the highest intensity true gaussian profiles, while the profiles fitted to lower intensity and larger σ data points, arising from the outer expanding rim, are fits to asymmetric and/or double peak line profiles. Figure 1 shows the quality of typical line profiles from each of the regions, displaying their intensity, central wavelength, and σ values.

3.2. Mrk 370

This BCD galaxy belongs to the Chained morphological type (see Cairós et al. 2001), in which the star formation takes place along a privileged direction. It follows the same star formation law as Mrk 324, with 25 young and massive exciting clusters hosted over an underlying stellar component with ages larger than 5 Gyr, (see Cairós et al. 2002). The clusters have an average age of 6.6 Myr with a dispersion of 0.9 Myr, suggesting a coeval and global star formation event. For the ones located in the inner nuclear region, the stellar mass content reaches up to several 10^5 $M_\odot$, (see Martínez-Delgado et al. 2006).

Figure 2 displays similar diagnostic diagrams for Mrk 370. The last frame in the upper row of panels shows the Hα image of the chained galaxy (see Cairós et al. 2001) obtained at the CAHA 2.2m telescope of the Centro Astronómico Hispano Alemán (CAHA), from Calar Alto Observatory (Spain). The ionized gas in Mrk 370 (see the Hα image in Figure 2) presents much more structure than Mrk 324. However, its σ *vs* I_{peak} diagram looks almost identical to that shown in Figure 1 for Mrk 324. The only exception is perhaps the low intensity data points with values of σ below the supersonic lower limit imposed by the horizontal band ($\leq$ 21 km s^{-1}, see first panel in Figure 2). The structure of the photoionized gas in Mrk 370 begins to be disentangled when one selects the data from the horizontal band in the σ *vs* I_{peak} diagram (see Figure 2, second row of panels). Such a data set appears clumped at three different λ_c values in the σ vs λ_c diagram. The brightest one sits at the rest wavelength of the galaxy (6580.1Å). There is a second one at ∼6579.4Å and a third one between these two at ∼6579.8Å. Two of them are much more apparent in the λ_c *vs* I_{peak} diagram where they clearly end up as pointed structures with different intensity (factors of 2) and different central wavelengths. The emission-line peak intensity map tracing the selected points (last frame in the second row) shows two major bursts of stellar formation and two adjacent much less intense, associated to the massive central stellar clusters with masses that range between $(8-50)\times10^4$ $M_\odot$ (see Martínez-Delgado 2005; Martínez-Delgado et al. 2006), also resolved by Cairós et al. (2002) using the INTEGRAL spectrograph with a single gaussian fit to the emission lines. All of these, although near the center of the galaxy, are kinematically resolved

as well detached structures. This multiplicity of structures would have been missed if one had only use the σ *vs* I_{peak} diagram as a diagnostic for this galaxy (see first panel in Figure 2), as the brightest points present almost the same supersonic gaussian profiles. These massive regions also match the area of the galaxy that shows the highest ionization values (see the Hα emission-line and the [OIII]/Hβ maps in Cairós et al. 2002).

The third row of panels in Figure 2 displays the data from the inclined bands with low intensity and large σ values in the σ *vs* I_{peak} diagram. This data set, as the corresponding one in Mrk 324, presents a large range of values of λ_c, around the systemic velocity of the galaxy. The spread of the data is also noticeable in the λ_c *vs* I_{peak} plane. The bulk of the data arises from a large galactic volume shown in the emission-line peak intensity map as an expanding rim of gas around the main centers of star formation all over the galaxy. This is most intense around the nuclear starburst zone and although less intense, it is still noticeable around smaller bursts of stellar formation some 2 kpc away from the nuclear region.

The final row of panels show the low intensity and low velocity dispersion data from the σ *vs* I_{peak} diagram (see Figure 2), which appears as vertical well detached low σ structures in the σ *vs* λ_c plane. These structures, given their low values of σ, detach well from the bulk of the data, most of which presents supersonic values, and due to their largely different λ_c values they also appear as well detached entities along the λ scale. Note however that given their low intensity values, they are much less apparent in the λ_c *vs* I_{peak} diagram. These data points correspond in the emission-line peak intensity map (last panel in the 4^{th} row of Figure 2) to multiple knots of emitting gas, or H II regions excited by low mass stellar groups (with masses $\leq 10^4$ $M_\odot$, see Martínez-Delgado 2005; Martínez-Delgado et al. 2006) at large distances from the centre of the galaxy. The line profiles arising from these regions are also gaussian profiles although with a very low intensity when compared to those arising from the central starburst regions (see inserts in the last frame of Figure 2).

3.3. III Zw 102

This galaxy is believed to be the result of an interaction event (see Vorontsov-Velyaminov 1959; Vorontsov-Vel'Yaminov 1977) and has been considered by some authors to belongs to the polar-ring galaxy type (Whitmore et al. 1990). It is morphologycally considered as an Extended Blue Compact Galaxy (Cairós et al. 2001), in which 65 star-forming regions were identified spreaded over the whole main body of the galaxy, including the arms. The age of the knots and their low age dispersion (6.1 ± 0.6 Myr) suggest a coeval starburst event (see Martínez-Delgado et al. 2006).

Figure 3 displays the results for III Zw 102. The last frame in the upper row of panels, shows the Hα image of the extended galaxy (see Cairós et al. 2001) obtained at the NOT 2.52m telescope of the Roque de Los Muchachos Observatory (ORM) in La Palma (Spain).

The data for III Zw 102 confirms the power of all of the diagnostic diagrams here used. The galaxy has a plethora of small H II regions spread along two arms as well as several massive centers of stellar formation in the densest nuclear region with masses between $\sim 10^5 - 10^6$ $M_\odot$, (see Martínez-Delgado 2005; Martínez-Delgado et al. 2006). All of these, as well as the large galactic volumes undergoing a supersonic expansion leave their signature in the diagnostic diagrams. In this way, the horizontal band with supersonic σ values at all possible intensities noticeable in the σ *vs* I_{peak} diagram (see Figure 3, 2^{nd} row of panels) is spread over a large range of λ_c values in the σ *vs* λ_c diagram and into at least four pointed structures (at λ_c = 6596.7Å, 6597.25Å, 6598Å, and 6600Å) of different intensities in the λ_c *vs* I_{peak} diagram. All of these in the emission-line peak intesity map are well resolved as giant structures within the galactic nuclear region. On the other hand, the larger σ points at all peak intensities in the σ *vs* I_{peak} diagram arise from gas expanding around the nuclear zone (see third row of panels in Figure 3). Among this data set is the inclined structure between I_{peak}=1100-1400 which is produced by gas between the four major centers of stellar formation in the nuclear region. The broad line structure appears at the center of the galaxy with a λ_c very similar to the systemic velocity of III Zw 102.

Finally, the lowest σ and lowest intensity data points in the σ *vs* I_{peak} diagram (last row of panels in Figure 3) appear, as in the case of Mrk370, as a set of well detached vertical stalactites in the σ *vs* λ_c diagram, hanging from the bulk of the data at very distinct λ_c values. The latter as shown in the last panel are produced by the numerous small H II regions located along the galactic arms. As shown by the inserts in the last column of panels, the quality of the gaussian fits is totally different in the three regions. The nuclear zone shows supersonic perfect gaussians while the surrounding gas presents much broader and asymmetric lines. Single gaussians with small σ values fit well the data from small centers of star formation.

4. Summary

Tridimensional spectroscopy with good spatial and spectral resolution, sampling a particular emission line over the whole area covered by an emitting nebula, is known to be the most suitable observational technique for analyzing the global kinematics of GHIIRs. In particular if a single gaussian fit is carried out over the emission lines in every pixel and from those, one infers the velocity dispersion, the central wavelength, and the peak intensity of the lines. The resultant σ *vs* I_{peak} diagram (Muñoz-Tuñón et al. 1996) has been shown to

be an excellent diagnostic diagram to separate the main broadening mechanisms affecting the emission lines, e.g., those that lead to shells and loops generated by the violent action from massive stars (see Dyson 1979, Roy et al. 1986) which finally lead to cloud dispersal, and the one(s) affecting the regions of massive star formation (either gravity; see Terlevich & Melnick 1981, Tenorio-Tagle et al. 1993, or turbulence; see Chu & Kennicutt 1994). The sequences shown by the various GHIIRs so far analyzed, led the authors also to propose the σ-I_{peak} plot as a tool able to trace the evolutionary status of a GHIIR, from its formation to the total dispersal of the ionized gas.

Here we have confirmed that the data from the inclined supersonic bands in the σ *vs* I_{peak} diagrams are caused by the mechanical energy deposited by massive stellar sources. These, depending on the age of the stellar clusters and on the density of the surrounding gas may affect small or large galactic volumes. However in all cases, the interaction leads to very asymmetric line profiles, evident in the σ *vs* I_{peak} diagram for their highly supersonic σ values.

Here we have extended the analysis to Blue Compact Galaxies. We have selected sources with a single nuclear starburst (as Mrk 324) as well as galaxies with multiple stellar bursts both within their nuclei as well as at large galactocentric distances. In all cases the σ *vs* I_{peak} diagram resembles those from GHIIRs in which the data define a supersonic σ (larger than $c_{\rm H\,II} \approx 10$ km s^{-1}) horizontal band with all possible intensity values. Note that the value of the limiting σ is different in every case. For III Zw 102 the horizontal band peaks at ~ 33 km s^{-1}, while for Mrk 324 and Mrk 370 it occurs at 24 and 25 km s^{-1}, respectively.

The σ horizontal band, for the case of multiple massive nuclear bursts of stellar formation, has been shown to split into different bands in the λ_c *vs* I_{peak} diagram. In this new diagram, the largest nuclear regions of massive star formation become evident due to the good spectral resolution. And thus even with a poor spatial resolution, or when dealing with further away sources, the sampling of the velocity field, with our 3D spectrographs, would reveal the exciting sources. Similarly, the σ *vs* λ_c new diagram picks up the small bursts of stellar formation by tracing their lower intensity and slower expansion of their immediate surroundings.

The stalactites detected in the σ *vs* λ_c diagram in the case of III Zw 102 and Mrk 370 correspond to the ionized knots located in the outskirts of the galaxies and their spread in σ result from the H II regions expansion into a low density medium (see Franco et al. 1990).

On the whole, the new diagnostic diagrams here presented provide the possibility of inferring from 3D spectroscopy, the magnitude of the star formation activity of distant galaxies, even if these are not spatially resolved.

IMD acknowledges the FPI grant (FP-2001-2506) of the Spanish Government through the collaboration of the project AYA2004-08260-C03-01 (ESTALLIDOS, http://www.iac.es/project/GEFE/estallidos). AVM acknowledges the the Russian Foundation for Basic Research (project 05-02-16454). This work is partly based on observations carried out at the 6m telescope of the Special Astrophysical Observatory of the Russian Academy of Sciences, operated under the financial support of the Science Department of Russia (registration number 01-43), and it has been partly supported by the ESTALLIDOS Project (AYA2004-08260-C03-01) and the grant AYA 2004-02703 from the Spanish Ministerio de Educación y Ciencia.

REFERENCES

Afanasiev, V. L., & Moiseev, A. V. 2005, Astronomy Letters, 31, 194

Cairós, L. M., Caon, N., Vílchez, J. M., Gónzalez-Pérez, J. N., & Muñoz-Tuñón, C. 2001, ApJS, 136, 2

Cairós, L. M., Caon, N., García-Lorenzo, B., Vílchez, J. M., & Muñoz-Tuñón, C. 2002, ApJ, 577, 164

Chu, Y.-H., & Kennicutt, R. C. 1994, ApJ, 425, 720

Dyson, J. E. 1979, A&A, 73, 132

Franco, J., Tenorio-Tagle, G., & Bodenheimer, P. 1990, ApJ, 349, 126

Fuentes-Masip, O., Muñoz-Tuñón, C., Castañeda, H. O., & Tenorio-Tagle, G. 2000, AJ, 120, 752

Martínez-Delgado, I., 2005, DEA: Catalogues and Parameters of Starburst Knots in a Sample of Blue Compact Dwarf Galaxies. *Spain: University of La Laguna/Instituto de Astrofíca de Canarias.*

Martínez-Delgado, I., Muñoz-Tuñón, C.,, Cairós, L. M., Tenorio-Tagle, G. 2006, *submitted to* AJ.

Moiseev, A. V. 2002, Bull. Special Astrophys. Obs., 54, 74

Muñoz-Tuñón, C., 1994, Violent Star Formation: From 30 Doradus to QSOs. *In: Tenorio-Tagle G. (eds.). Cambridge University Press, p.25.*

Muñoz-Tuñón, C., Gavryusev, V., & Castañeda, H. O. 1995, AJ, 110, 1630

Muñoz-Tuñón, C., Tenorio-Tagle, G., Castañeda, H. O., & Terlevich, R. 1996, AJ, 112, 1636

Roy, J.-R., Arsenault, R., & Joncas, G. 1986, ApJ, 300, 624

Sabalisck, N. S. P., Tenorio-Tagle, G., Castañeda, H. O., & Muñoz-Tuñón, C. 1995, ApJ, 444, 200

Telles, E., Muñoz-Tuñón, C., & Tenorio-Tagle, G. 2001, ApJ, 548, 671

Tenorio-Tagle, G., Muñoz-Tuñón, C., & Cox, D. P. 1993, ApJ, 418, 767

Terlevich, R., & Melnick, J. 1981, MNRAS, 195, 839

Thuan, T. X., & Martin, G. E. 1981, ApJ, 247, 823

Vorontsov-Velyaminov, B. A. 1959, VV, 0

Vorontsov-Vel'Yaminov, B. A. 1977, A&AS, 28, 1

Whitmore, B. C., Lucas, R. A., McElroy, D. B., Steiman-Cameron, T. Y., Sackett, P. D., & Olling, R. P. 1990, AJ, 100, 1489

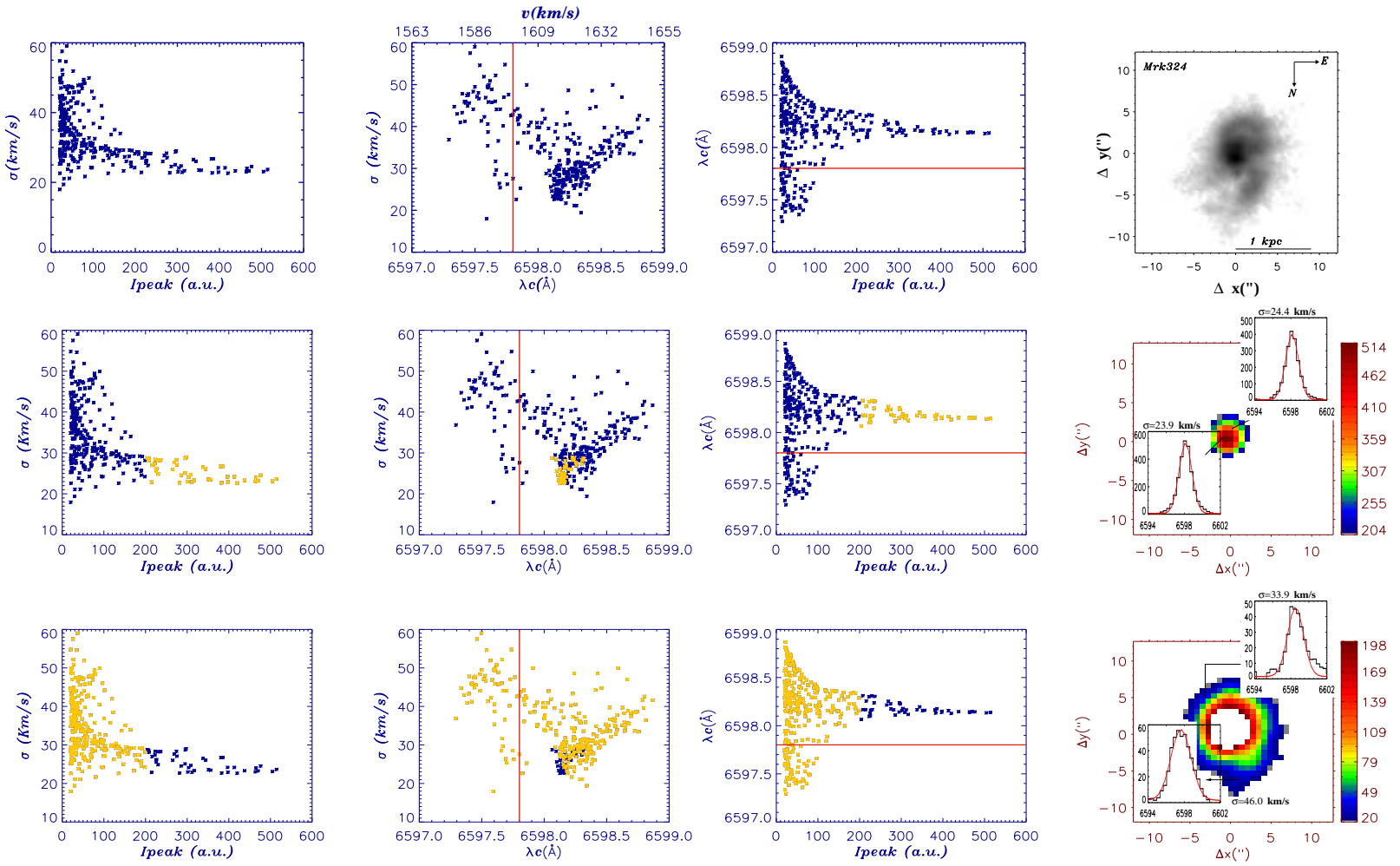

Fig. 1.— The figure shows in the first row of panels the velocity dispersion σ *vs* peak intensity (the σ was corrected for the instrumental and thermal broadening), for all the gaussian fits to the individual spectra of Mrk 324. The second and third panels display the corresponding σ *vs* central lambda (λ_c, indicating also the velocity range in km s^{-1}) and λ_c *vs* peak intensity, respectively. The solid line in these two panels indicates the rest velocity of the galaxy. The last panel shows the Hα image of the galaxy and indicates its scale in kpc. The second and following rows of panels highlight in colour the various sets of data points selected in the σ *vs* peak intensity diagram and their location in the σ *vs* λ_c and λ_c *vs* peak intensity planes. The last panels in every row, with a peak intensity scale, display the locations in the galaxy that produce the selected data points. Inserts in these panels correspond to typical gaussian fits (solid red lines) to the data arising from different regions (axis correspond to intensity, in counts, vs the wavelength in Å). The fitted σ values are indicated in every frame.

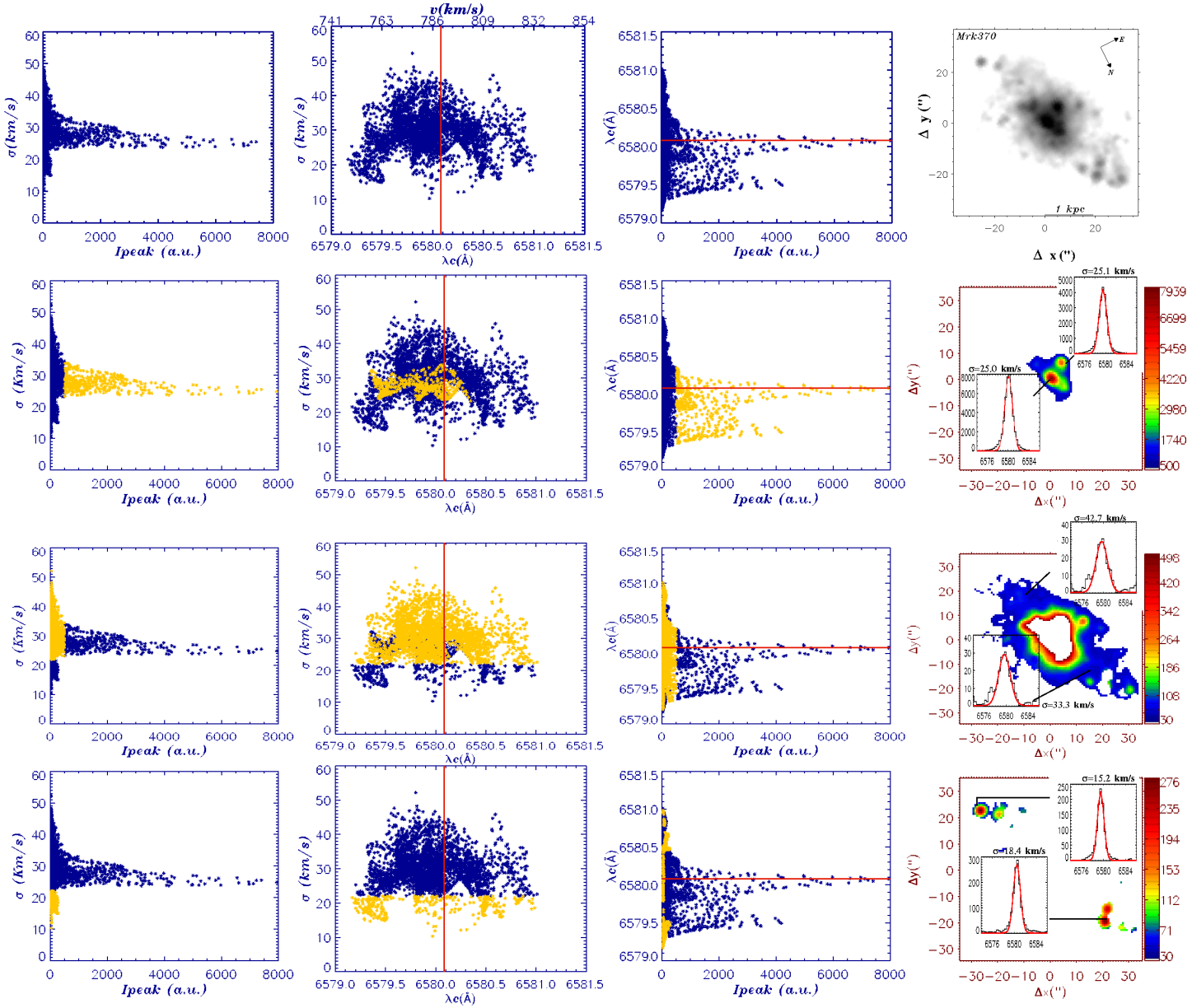

Fig. 2.— Mrk 370. The same as Figure 1 for Mrk 370.

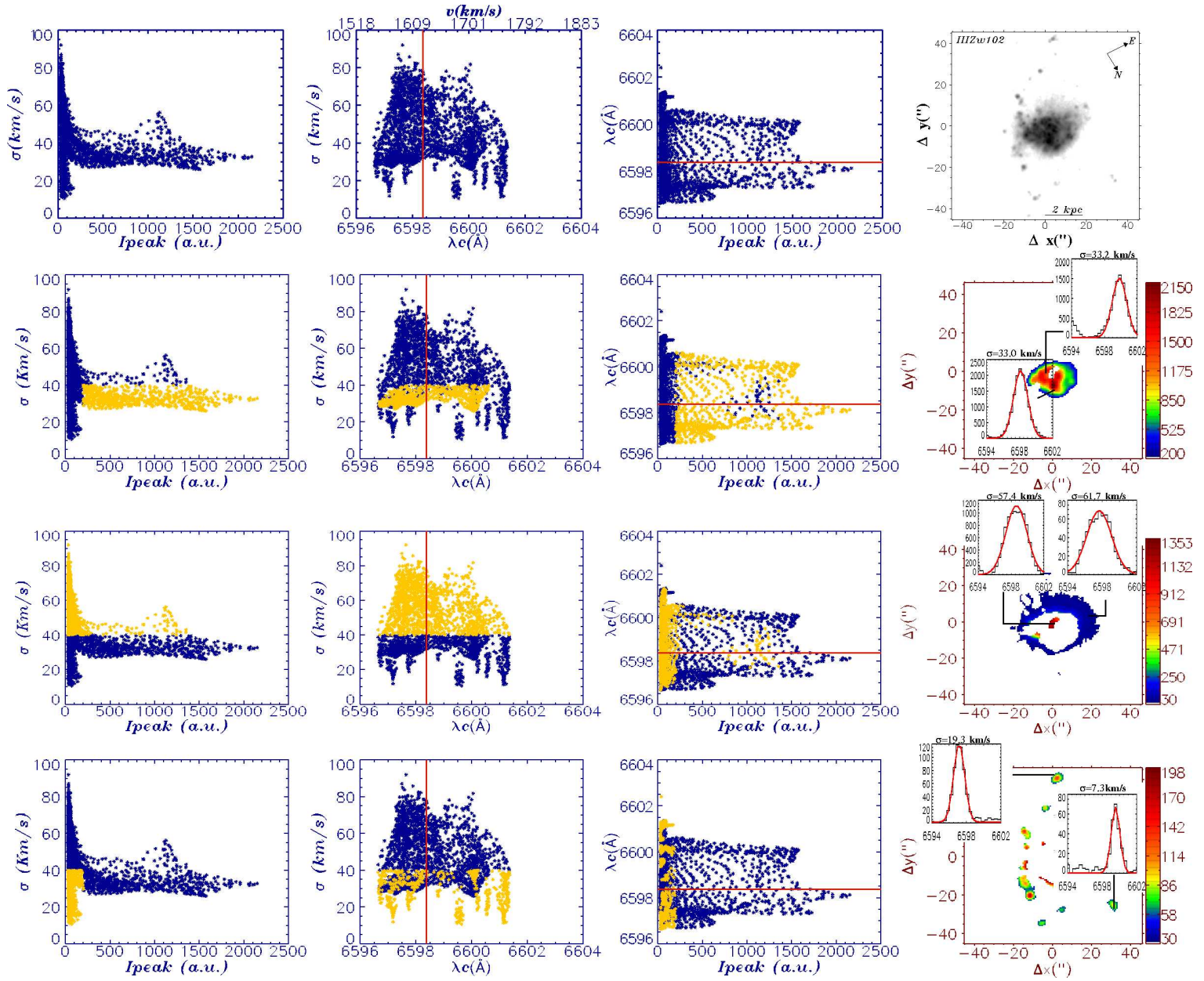

Fig. 3.— III Zw 102. The same as Figure 1 for III Zw 102.

Table 1. Log of the Observations

Galaxy (1)	RA(2000) (2)	DEC(2000) (3)	Linear Scale(pc/″) (4)	t(s) (5)	PSF(″) (6)	V_{HI}(km s^{-1}) (7)	D(Mpc) (8)
Mrk370	$02^h40^m29\overset{s}{.}0$	$+19°17'50''$	52	4680	1.7	790†	10.85
IIIZw102	$23^h20^m30\overset{s}{.}1$	$+17°13'32''$	110	6480	1.8	1626†	22.71
Mrk324	$23^h26^m32\overset{s}{.}8$	$+18°15'59''$	108	4320	1.6	1600†	22.43

†Systemic velocity, from H I observations, corrected to the Local Group velocity centroid taken from Thuan & Martin (1981).